

# Catalysis Science & Technology

Accepted Manuscript

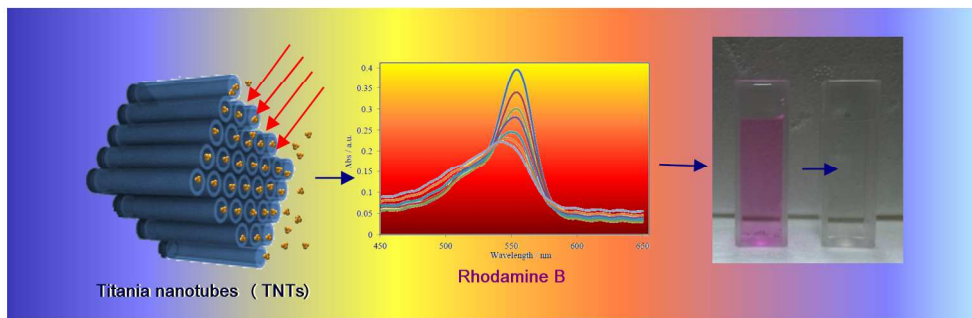


This is an *Accepted Manuscript*, which has been through the Royal Society of Chemistry peer review process and has been accepted for publication.

*Accepted Manuscripts* are published online shortly after acceptance, before technical editing, formatting and proof reading. Using this free service, authors can make their results available to the community, in citable form, before we publish the edited article. We will replace this *Accepted Manuscript* with the edited and formatted *Advance Article* as soon as it is available.

You can find more information about *Accepted Manuscripts* in the [Information for Authors](#).

Please note that technical editing may introduce minor changes to the text and/or graphics, which may alter content. The journal's standard [Terms & Conditions](#) and the [Ethical guidelines](#) still apply. In no event shall the Royal Society of Chemistry be held responsible for any errors or omissions in this *Accepted Manuscript* or any consequences arising from the use of any information it contains.



822x277mm (72 x 72 DPI)

Cite this: DOI: 10.1039/c0xx00000x

ARTICLE TYPE

www.rsc.org/xxxxxx

## Influence of dimensions, inter-distance and crystallinity of titania nanotubes (TNTs) on their photocatalytic activity

Mohammed Alsawat,<sup>a</sup> Tariq Altalhi,<sup>a</sup> Joe G. Shapter<sup>b</sup> and Dusan Losic<sup>a,b</sup>

Received (in XXX, XXX) Xth XXXXXXXXX 20XX, Accepted Xth XXXXXXXXX 20XX

DOI: 10.1039/b000000x

### Abstract

The aim of this study is to explore the influence of structural parameters of titania nanotubes (TNTs) including pore diameters, length, nanotube inter-distance and crystallinity on their photocatalytic properties. TNTs were prepared under various experimental conditions of applied potential, anodization time and the electrolyte water content. The morphology and crystalline structures of the prepared TNTs were characterized using scanning electron microscopy (SEM) equipped with energy dispersive X-ray spectroscopy (EDX), and X-ray diffraction (XRD). The results showed that the nanotube's length, diameters and nanotube inter-distance were significantly affected using different anodization conditions. The photocatalytic activities of the prepared TNTs were evaluated via the degradation of the Rhodamine B in aqueous solution under Mercury-Xenon Hg (Xe) lamp irradiation monitored by UV-visible spectroscopy. The influence of TNTs structural properties including tube's length, inter-tube distance and crystallinity on their photocatalytic activity were evaluated. It was found that TNTs with shorter and larger nanotube inter-distances have better degradation rates of Rhodamine B than long tubes. Moreover, the TNTs annealed at 650 °C to produce an anatase/rutile mixture (86.5 and 13.5% respectively) exhibited higher photocatalytic activity than other TNTs annealed at 250 °C, 450 °C, and 850 °C.

Keywords: Titania nanotubes; Anodization; Photodegradation; Rhodamine B

### 1. Introduction

Water shortage has become one of the top challenges facing societies worldwide in this century. The possibility of reusing water or purification of contaminated water is an attractive option to address this problem. Conventional water treatment technologies including chlorination, filtration and membrane technologies have been widely used to reduce the level of pollutants in water. However, some drawbacks of using these methods include the potential to generate secondary toxic pollutants, inability to degrade a variety of pollutants and high operating cost.<sup>1, 2</sup> Hence the development of new advanced technologies based on new materials and purification processes are urgently needed.

The advanced oxidation process (AOP) has been shown to be a promising solution to reduce existing water pollution and solve water shortage problems.<sup>3,4</sup> Photocatalysis is a process which uses light to activate a catalyst, usually a semiconductor, which can be activated by photons of appropriate energy to form electron-hole pair allowing to redox reactions to take place.<sup>4</sup> This process based on nano-catalysts has been used successfully in the degradation of a wide variety of contaminants.<sup>5</sup> It was found that

the specific surface area plays a major role in the photocatalysis using nano-catalysts providing more adsorption and catalytic sites for photocatalytic reactions.

Among the various photocatalysts, nanosized titanium dioxide (TiO<sub>2</sub> or titania) has attracted considerable attention due to its unique properties including low cost fabrication, large specific surface area, chemical stability, non-toxicity and high photocatalytic activity. The titania nanostructures have been synthesized by various approaches including a template method,<sup>6</sup> a sol-gel method,<sup>7</sup> a hydrothermal treatment<sup>8</sup> and an electrochemical anodization.<sup>9-11</sup> Electrochemical anodization of titanium based on self-ordering is demonstrated as one of most attractive approaches because it is a simple, inexpensive, self-driven and scalable process for creating titania oxide film with characteristic vertically aligned and highly ordered nanotubular or nanoporous structures.<sup>12,13</sup> Titania nanotube (TNT) arrays were extensively explored for broad applications with thousands papers and most attractive and promising are solar cells, drug delivery and biosensing.<sup>9,11</sup>

Several studies have successfully demonstrated the application of TNTs as a photocatalyst for the removal of chemical pollutants in the environment.<sup>9,14,15</sup> These studies confirmed that nanotubular geometry of TNTs have better photocatalytic activity

compared with spherical forms of TiO<sub>2</sub> powders or nanoparticles.<sup>16</sup> In order to improve and manipulate photocatalytic properties of TNTs the influence of crystallinity and the geometry of nanotube structures (length, the pore size) was studied showing to have an impact on their catalytic performance.<sup>17,18</sup> TNTs have unique structure with tightly and perpendicularly packed nanotubes and inter-distance between nanotubes with additional expose of external nanotube surface is expected to have impact on their photocatalytic performance.<sup>9-11</sup>

The chemical composition of inner of TNT surface as result of incorporation of ions from electrolyte is possible to have different composition from outer TNT surface including different catalytic properties. This issue is not explored yet, but it is important for many applications of TNTs where the both surfaces can be used as active reaction areas.

Hence the aim of this study is to synthesize TNTs with different nanotube's length, inter-tube distance and crystallinity using different anodization conditions and explore their influence on photocatalytic activity. The photocatalytic activity decomposition of organic pollutants was investigated using Rhodamine B as a model organic molecule. The degradation rate of Rhodamine B using different TNTs substrates under UV illumination was performed in aqueous solution using UV-Vis spectroscopy in order to determine key structural parameters which determines photocatalytic properties of TNTs.

## 2. Experimental details

### 2.1. Materials

Titanium foil (0.127 mm thickness, 99.7% purity) was purchased from Sigma-Aldrich. Ethylene glycol, ammonium fluoride (NH<sub>4</sub>F) and Rhodamine B were also obtained from Sigma-Aldrich. Deionized water (DI) was used throughout the experiments.

### 2.2. Fabrication of TNTs on Ti

The Ti foil was cut into small pieces of 15 mm × 15 mm and used as substrate to prepare TNTs by electrochemical anodization process. The Ti foil was mechanically polished by abrasive paper, and then degreased by sonicating in acetone, isopropanol and ethanol followed by rinsing with deionized (DI) water and drying with a nitrogen stream. For electrochemical anodization, a special electrochemical cell with two electrodes and computer-controlled power supply (Agilent) was used as previously reported<sup>19,20</sup>. Samples were contacted with a Cu back-plate in an electrode holder that permits only a circular area of Ti metal with diameter of 1 cm to be exposed to the electrolyte. This Ti served as the anode while platinum (Pt) foil was used as the cathode. TNTs were prepared through a two-step anodization process using electrolyte solution containing ethylene glycol with 0.3% NH<sub>4</sub>F and water content (1-3%). The first anodization step was performed under 100 V for 2 hours at room temperature. The resultant layer of TNTs was removed mechanically followed by sonicating in methanol. The second anodization step was performed under various voltages from 20 V to 100 V for different times from 20-80 minutes in order to investigate the influence of these parameters on the nanotube structure (diameters and length). After anodization, the samples were rinsed with DI water and dried in a nitrogen stream.

### 2.3. Characterization of TNTs samples

The surface morphology of the prepared TNTs samples was examined by FEG Environmental SEM (Quanta 450). EDX spectra were obtained to determine elemental composition of TNTs. Powder X-ray diffraction (XRD) method was used for crystal phase identification and estimation of the crystallite size. The XRD measurements were carried out at room temperature using a Rigaku MiniFlex 600 X-ray diffractometer operating with diffracted beam graphite monochromators (Cu K $\alpha$  with  $\lambda = 0.15406$  nm) at 40 kV and 15 mA. The crystalline size was calculated from the peak width using Debye Scherrer equation<sup>21</sup>:

$$D = K\lambda / (\beta \cos \theta) \quad (1)$$

Where  $K$  is a dimensionless constant (0.94),  $\theta$  is the diffraction angle,  $\lambda$  is the X-ray wavelength (1.54 Å), and  $\beta$  is the full-width at half-maximum (FWHM) in the  $2\theta$  scan (radians). The weight fractions of the anatase and rutile phases of the nanotubes was estimated based on the corresponding most intense peaks using the following equations,

$$W_A = [1 + 1.26 (IR / IA)]^{-1} \quad (2)$$

$$W_R = [1 + 0.8 (IA / IR)]^{-1} \quad (3)$$

where IA and IR are the X-ray integrated intensities of reflection of anatase and rutile respectively.<sup>22</sup>

### 2.4. Photodegradation experiments

The photocatalytic activity of the TNTs was evaluated via the photodegradation of the Rhodamine B in aqueous solution. The photodegradation experiments were carried out in glass beaker under a 1000 W Mercury-Xenon Hg (Xe) lamp irradiation. This type of lamp has spectral distribution that includes a continuous spectrum from the ultraviolet to infrared spectrum. The incident photon flux entering the photoreactor was  $9.1 \times 10^{-6}$  einstein cm<sup>-2</sup> s<sup>-1</sup>. The TNTs sample with diameter of 1 cm (8-10 mg) was placed in 10 ml of Rhodamine B aqueous solution with an initial concentration of 1.6 mg/L. Prior to the photoreaction, the TNTs sample was immersed in the Rhodamine B aqueous solution for 1 hour in dark area to reach adsorption/desorption equilibrium. After that, the reaction solution was irradiated vertically from the top by the Hg (Xe) lamp with a distance of 6 cm while slightly agitating the solution using a stirrer. After every 30 minutes of irradiation, a solution was taken and centrifuged for 3 minutes and the concentration of Rhodamine B was measured at absorbance of 554 nm. The degradation of Rhodamine B was monitored by UV-visible spectroscopy to calculate degradation efficiency through the equation:

$$\text{Degradation efficiency (\%)} = C_0 - C_t / C_0 \times 100 \quad (4)$$

Where: C<sub>0</sub>: Initial concentration of Rhodamine B.

C<sub>t</sub>: Rhodamine B concentration at time t (min).

As a control the irradiation of Rhodamine B without of TNTs was obtained. The photonic efficiency ( $\xi$ ) was calculated as the ratio of the initial photocatalytic degradation rate (mol L<sup>-1</sup> s<sup>-1</sup>) to the rate of incident photons entering the reactor (einstein L<sup>-1</sup> s<sup>-1</sup>)<sup>23</sup>.

## 3. Result and discussion

### 3.1. Structural characterization using SEM

A typical TNT structure produced through a two-step anodization process (at 100 V for 1 hour, 2<sup>nd</sup> anodization step) at 25 °C is shown in Fig. 1. The top view of the TNT's surface shows pores with diameters of  $120 \pm 10$  nm (Fig. 1a) with tight interconnection of nanotubes without of interspace. A cross-sectional image of the TNT is presented in Fig. 1b, which illustrates the very well ordered tubes oriented perpendicularly to the top surface of the Ti substrate with an average tube length of  $45 \pm 5$   $\mu$ m. These tubes closed ends as shown in the bottom view (Fig. 1c). EDX spectra of TNTs is presented in Fig. 1d showing characteristic X-ray energy level for Titanium (K = 4.510 keV and K = 4.931 keV) and oxygen (K = 0.523 keV) as a major elements of TNTs with percentage weight of 64 % and 27.2 % respectively. Carbon and nitrogen were presented with percentage weight of 4.3 % and 4.5 % respectively and their presence is related by adsorption ions from electrolyte (ethylene glycol with and NH<sub>4</sub>F)

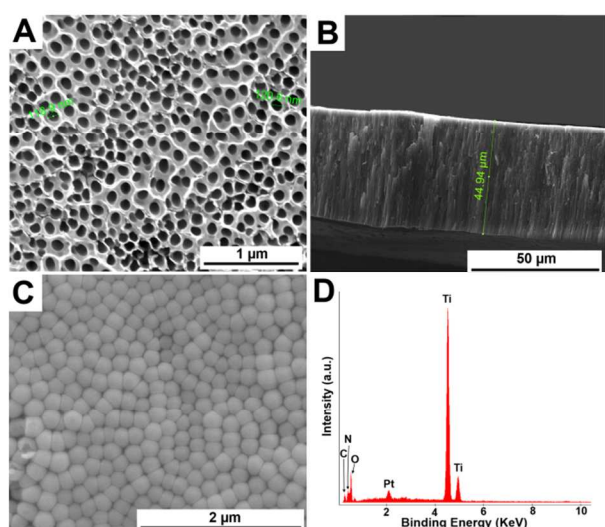


**Fig. 1** SEM images of the typical TNTs structure prepared through a two-step anodization process at 25 °C in electrolyte solution containing ethylene glycol with 0.3 % NH<sub>4</sub>F and 3 % water, (a) top view, (b) cross section and (c) bottom view (d) EDX spectra.

### 3.1.1. Controlling TNT dimensions by anodization voltage and time

To study the influence of the anodization voltage on the TNT structures, five experiments were conducted at 25 °C using the same anodization time (1hour) and different voltages 20 V, 40 V, 60 V, 80 V and 100 V all performed in the 2<sup>nd</sup> anodization step. Ti anodized at a low voltage of 20 V for 1 hour didn't show the growth of nanotubes. A partial porous structure was observed indicating that 20 V is not a sufficient voltage to grow nanotubes due to weak electrochemical oxidation and oxide dissolution process. Previous studies showed that only under sufficient applied potential titanium (Ti) are oxidized to Ti<sup>4+</sup> ion by an electric field to form oxide layer.<sup>9,11,24</sup> The strong electric field is also required for the dissolution of the formed oxide at the electrolyte/oxide interface important for the formation and growth of nanotube structure and their alignment on the Ti surface.<sup>24</sup> This is confirmed by our results where by increasing the anodization voltage from 40 V to 100 V, well aligned nanotubes were formed. Fig. 2 summarise the influence of TNT

pore diameters prepared by different anodization voltages (20–100 V) for 60 min. The graph indicates a linear increase of the pore diameters from 50 nm to 120 nm with anodization voltage (40 - 100V). These results confirm that the diameters of TNTs can be controlled by voltage which is in agreement with previous studies.<sup>9-11</sup> However it is important to state that the anodization voltage also has influence on the growth rate on TNTs. The TNTs with different length of  $5 \pm 1.6$   $\mu$ m,  $10 \pm 2.5$   $\mu$ m,  $20 \pm 2.3$   $\mu$ m,  $45 \pm 3.3$   $\mu$ m were obtained for 60 min using voltages 40V, 60V, 80V and 100 V respectively (Fig 2). Therefore to prepare TNTs with desired pore diameters and length it is necessary to consider growth rate at different voltage and anodization time.

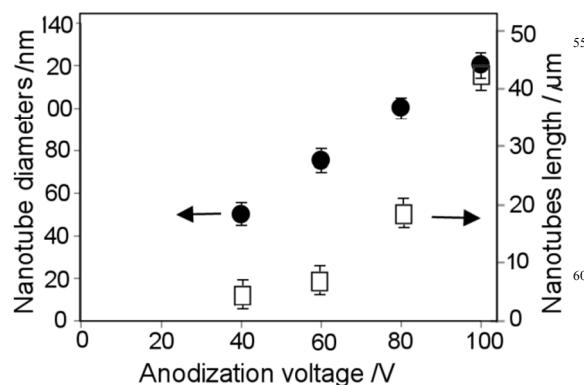


**Fig. 2** The controlling inner diameters and length of TNTs using different anodization voltages (20V-100V, two step anodization, electrolyte composition of 0.3% NH<sub>4</sub>F and 3% water) and constant anodization time (60 min)

To study the influence of the anodization time on the TNT structures, four experiments were conducted at 100 V using anodization times of 20 min, 40 min, 60 min and 80 min. Results are summarized in Fig. 3 showing the changes of nanotube lengths and nanopore diameters. It was observed that the length of TNTs was increased with increasing of the anodization time showing a linear relationship showing average growth rate of 0.6  $\mu$ m/min. The lengths of the TNTs prepared by for 20 min, 40 min, 60 min and 80 min were about 9  $\mu$ m, 19  $\mu$ m, 45  $\mu$ m and 50  $\mu$ m respectively. The anodization time also has influence on pore

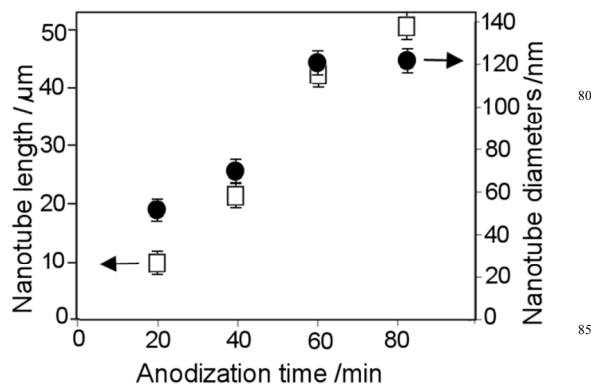


**Fig. 3** The controlling length and inner diameter s of TNTs using different anodization time (20-80min, two step anodization process electrolyte composition of 0.3 % NH<sub>4</sub>F and 3 % water) and constant anodization voltage (100 V).

diameters showing increased TNTs diameters from of 50 nm to 120 nm. These results confirm that the anodization time can be used as a simple parameter for controlling TNTs length. By controlling voltage both the length and pore diameters can be precisely tuned to values required for specific applications. The prepared TNTs with different dimensions with and without of thermal treatment were explored in following study to determine their influence on catalytic performance.

### 3.1.3. Influence of electrolyte water content

To study the influence of the electrolyte water content on the structure of the nanotubes, an experiment was conducted with reducing the electrolyte water content from 3 % to 1 % with the same anodization conditions (100 V for 60 min for the 2<sup>st</sup> anodization at 25 °C). The SEM images of prepared TNTs showing the top, cross-section and bottom surface is presented in Fig.4. These images show that the tube's length and inner diameter were significantly influenced with decreasing the water content from 3 % to 1 %. It was found that the length and the inner diameter of the TNTs prepared in electrolyte solution containing 1% of water were decreased to  $16.9 \pm 5 \mu\text{m}$  and  $46.2 \pm 10 \text{ nm}$  compared to  $45 \pm 1.1 \mu\text{m}$  and  $120 \pm 2.3 \text{ nm}$  prepared using 3 % of water in electrolyte. Furthermore, the inter-tube distance and voids between nanotubes were increased compared with TNTs prepared in 3 % water (Fig.1) as a result of reducing water content as it is shown in the top and bottom views in Fig. 4a,c respectively. The scheme of TNTs larger inter-distance is presented in Fig. 4d. These results clearly indicate that water content plays a major role in the nanotube growth rate and by controlling water contents it is possible to make TNTs with controllable inter-distances. Water is acting as a source of  $\text{H}^+$  and  $\text{O}^{2-}$  ions required for the formation of oxide layer and hence increasing the water content leads to increasing the growth rate and tube's length. This anodization condition, which provides TNTs with characteristic large inter-space between nanotubes is used to explore influence of external TNTs surface and increased surface area on their catalytic properties.

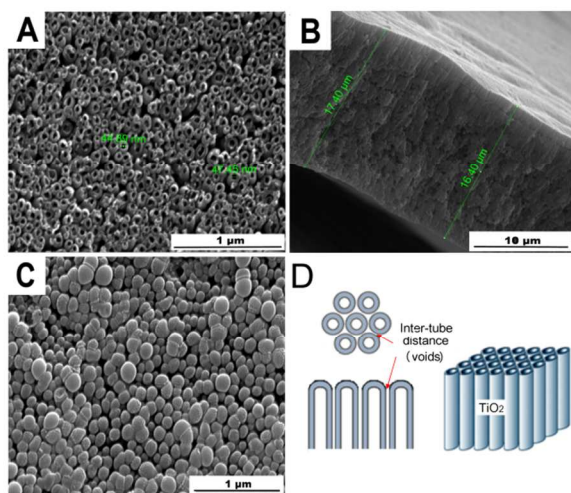


**Fig. 4** SEM images of the TNTs prepared in electrolyte solution containing 1% of water at 25 °C showing a) the top view, b) cross-section and c) the bottom view. d) scheme of the inter-tube distance and voids increased using this anodization conditions.

### 3.1.4. XRD characterization of annealed TNTs

A crystalline structure of  $\text{TiO}_2$  is highly desired in photocatalytic applications since it eliminates defects of the amorphous nature and improves their catalytic properties<sup>25</sup>. TNTs as produced are amorphous and to crystallize them it is required to perform annealing TNTs at different temperatures. The XRD patterns obtained for TNTs after annealing at different temperatures (250 °C, 450 °C, 650 °C and 850 °C) in a dry oxygen atmosphere are shown in Fig. 5. These patterns were compared to the XRD data obtained from the database<sup>26</sup>. The TNTs as produced (25 °C) showed broad peak indicating the amorphous phase. The XRD peaks obtained at an annealing temperature of 250 °C correspond to the anatase phase of  $\text{TiO}_2$  (JCPDS CAS No. 21-1272). These peaks were observed at  $2\theta = 25.2^\circ$  (101),  $37.5^\circ$  (004),  $47.8^\circ$  (200),  $53.5^\circ$  (105),  $55^\circ$  (201),  $62.3^\circ$  (213) and  $75^\circ$  (215). The intensity of these peaks increased with increasing annealing temperatures to 450 °C and 650 °C. The presence of these peaks and the absence of a rutile phase peaks at 250 °C and 450 °C is an indication of the successful production of the anatase  $\text{TiO}_2$  phase. A rutile type  $\text{TiO}_2$  (13.5%) was clearly observed based on peaks appearing at  $2\theta = 27.5^\circ$  (110),  $36^\circ$  (101) and  $41.1^\circ$  (111) in the sample that was annealed at 650 °C. When the annealing temperature was increased to 850 °C, these peaks become more pronounced and a further rutile peak appears at  $54.2^\circ$  (211). These results clearly indicate that 450 °C is the optimal annealing temperature for

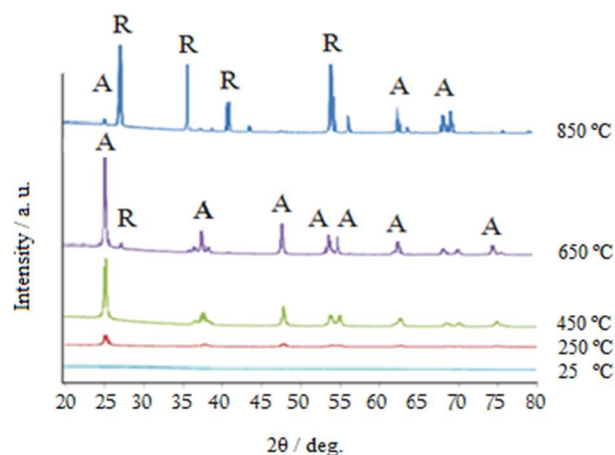


**Fig. 5** XRD patterns of as produced TNTs (25 °C) and after annealing at different temperatures (250 °C, 450 °C, 650 °C and 850 °C).

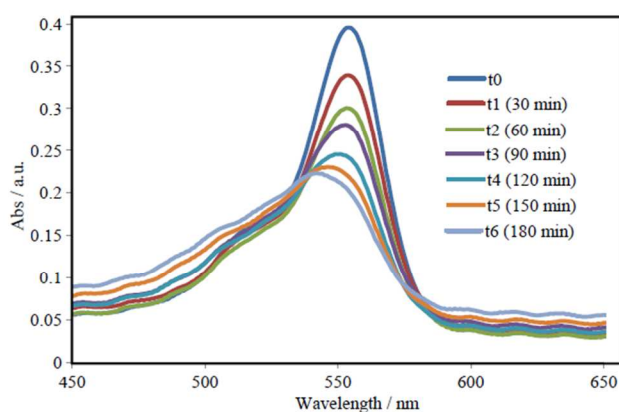
getting exclusively anatase phase of  $\text{TiO}_2$ . Increasing the temperature over 450 °C leads to the conversion from thermodynamically metastable anatase phase to the more stable rutile phase. Table 1 lists the calculated values of average crystalline sizes and phase composition of TNT samples annealed at different temperatures, using equations (1, 2 and 3 in experimental details section). TNTs samples annealed at 250 and 450 °C have only anatase phase of  $\text{TiO}_2$  (100 %) while TNT sample annealed at 650 °C has anatase/rutile mixture (86.5 % and 13.5 % respectively). The conversion from anatase to rutile phase of  $\text{TiO}_2$  becomes more pronounced by increasing the temperature to 850 °C (12.1 % anatase and 87.9 % rutile).

**Table 1** The phase composition and average crystal size and of the annealed TNTs using different temperatures

Annealed TNTs (°C)	Average crystal size (nm)		Phase composition (%)	
	Anatase	Rutile	Anatase	Rutile
250	21.3	-	100	-
450	23.6	-	100	-
650	32.7	45	86.5	13.5
850	53.1	65.7	12.1	87.9

### 3.2. Photodegradation study using TNTs with different nanotube dimensions

The photocatalytic activity of the prepared TNTs was evaluated via the degradation of the Rhodamine B in aqueous solution under Mercury-Xenon Hg (Xe) lamp irradiation. The notable decrease in the Rhodamine B absorbance in the presence of TNTs prepared through a two-step anodization process (the length of 45  $\mu\text{m}$ ) is shown in Fig. 6. It confirms that TNTs can catalyze the degradation of Rhodamine B in the presence of light. The decrease in the absorbance was accompanied by a shift in the absorbance peak position from 554 nm to 542 nm which is a result of the formation of intermediate products.<sup>27</sup> The TNTs without of annealing (as prepared at 25 °C) had degraded about only 44.2 % of the Rhodamine B within 180 minutes (Table 2). This low degradation rate is due to the amorphous structure of as prepared TNTs. Although an amorphous phase of TNTs has a large surface area which plays a major role in the photocatalysis process, it has a low photoactivity because of the high number of surface defects, which act as recombination centres for the electrons and holes, and low crystallinity.<sup>12,28</sup>

**Fig. 6** Typical absorption spectra of degradation Rhodamine B aqueous solution in the presence of TNTs (45  $\mu\text{m}$  long) under Hg (Xe) light irradiation.

#### 3.2.1. Kinetic study

Previous studies have shown that the photodegradation of Rhodamine B over illuminated  $\text{TiO}_2$  particles follows the Langmuir–Hinshelwood (L–H) kinetics model:

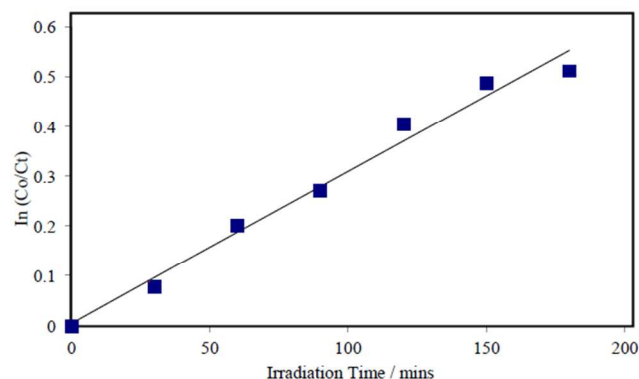
$$r = \frac{dC}{dt} = \frac{kKC}{1 + KC} \quad (5)$$

Where  $r$  is the oxidation rate of the reactant ( $\text{mg/l min}$ ),  $C$  is the

concentration of the reactant ( $\text{mg/l}$ ),  $t$  is the illumination time,  $k$  is the reaction rate constant ( $\text{mg/l min}$ ), and  $K$  is the adsorption coefficient of the reactant ( $\text{l/mg}$ ). Equation (5) can be simplified to first-order equation when the initial concentration is small:

$$\ln(C_0/C) = kt \quad (6)$$

Where  $k$  is the rate constant,  $C$  is the concentration,  $C_0$  is the concentration at  $t = 0$ <sup>29-31</sup>.

**Fig. 7** The semi-log graph of the degradation of Rhodamine B TNTs (45  $\mu\text{m}$  long) under Hg (Xe) light irradiation

In this study, the semi-log graph of the Rhodamine B concentration versus irradiation time gave a straight line was observed (Fig. 7) indicating the pseudo-first-order reaction. The slope of the linear regression equals the first order rate constant. The degradation reaction using 45  $\mu\text{m}$  long TNTs had rate constant ( $k$ ) of  $3 \times 10^{-3} \text{ min}^{-1}$ . The correlation coefficient ( $R^2$ ) value is around 0.98 which indicating excellent linear reliability.

#### 3.2.2. Influence of the TNTs structure on photodegradation performance

The degradation results of Rhodamine B solution in the presence of TNTs with two different lengths (45  $\mu\text{m}$  and 10  $\mu\text{m}$ ) are presented in Figure 8 to show the influence of TNTs length on their photocatalytic activity. It was found that the 10  $\mu\text{m}$  long TNTs exhibited a considerable enhancement in the degradation rate of the Rhodamine B over the 45  $\mu\text{m}$  long TNTs. The 10  $\mu\text{m}$  long TNTs degraded 67.5% of the Rhodamine B within 180 minutes versus 44.2% of the 45  $\mu\text{m}$  long TNTs (Table 2). It is generally known that long nanotubes have a high photocatalytic activity for the degradation of dyes based on the fact that they provide more active sites for the adsorption of the dyes on their surfaces. However, the result here indicates that short tubes have higher photocatalytic activity than long tubes likely due to two factors. One is the diffusion of Rhodamine B molecules and the second is the incidents of photons which are more efficient inside shorter nanotubes. On the other hand, long nanotubes have limited penetration depth of the incident photons which affects the diffusion of the reactant inside the tubes and in turn negatively affected the photocatalytic activity<sup>32</sup>. The conclusion is that dimensions of TNTs needs to be optimised regarding these two parameters.

To study the influence of the inter-tube distance, two

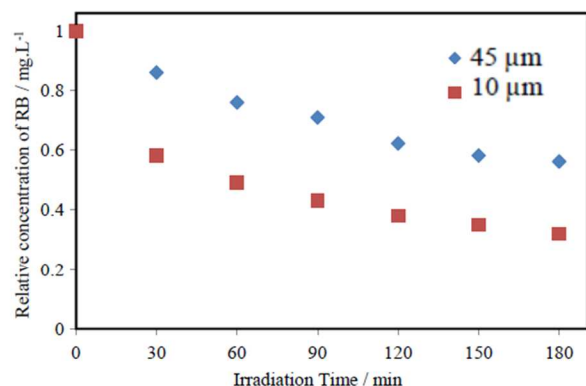


**Fig. 8** The influence of the length of TNTs (45  $\mu\text{m}$  and 10  $\mu\text{m}$ ) on their photodegradation properties and removal of Rhodamine B

**Table 2** Summary of the degradation of the Rhodamine B with TNTs samples with different nanotube dimensions and crystallinity

TNTs/ Length/ H <sub>2</sub> O%	Temp. (°C)	Degradation RB (%)	Time (min)	Rate constant (min <sup>-1</sup> )	Photonic efficiency (%)
17 $\mu\text{m}$ , 1%	25	75.9	180	$7.8 \times 10^{-3}$	1.069
10 $\mu\text{m}$ , 3%	25	67.5	180	$5.3 \times 10^{-3}$	0.726
45 $\mu\text{m}$ , 3%	25	44.2	180	$3 \times 10^{-3}$	0.411
45 $\mu\text{m}$ , 3%	250	100	150	$1.4 \times 10^{-2}$	1.92
45 $\mu\text{m}$ , 3%	450	100	120	$1.8 \times 10^{-2}$	2.468
45 $\mu\text{m}$ , 3%	650	100	90	$2.3 \times 10^{-2}$	3.154
45 $\mu\text{m}$ , 3%	850	51.6	180	$4 \times 10^{-3}$	0.548

photodegradation experiments were tested with a TNTs sample that does not have space between tubes, which prepared by the standard water content 3 %, and TNTs sample that has space between tubes, which prepared by reducing the water content to 1 %. Degradation results for Rhodamine B using these two samples are presented in figure 9. TNTs prepared by 1 % water showed

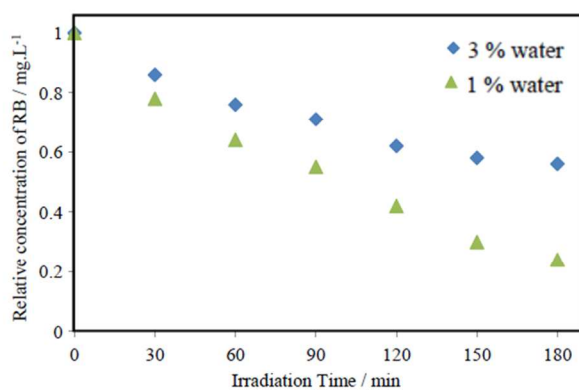


**Fig. 9** The influence of nanotube inter-distance on photocatalytic performances demonstrated by removal of Rhodamine B under Hg (Xe) light irradiation using TNTs produced with electrolyte with 3 % (tightly packed TNTs) and 1 % water (large voids between nanotubes).

better degradation rate of Rhodamine B than TNTs prepared by 3 % water. TNT prepared by 1 % water degraded about 75.9 % of the Rhodamine B within 180 minutes versus 44.2 % by TNTs

prepared by 3 % water (Table 2). This enhancement in the degradation rate is explained by the fact that the space between tubes provides more catalytic sites for the adsorption of the Rhodamine B molecules using both the inner and the outer surface of TNTs. It should be mentioned that these two types of TNTs samples have slightly different in lengths (45  $\mu\text{m}$  for 3 % water versus 16.9  $\mu\text{m}$  1 % water). However, when comparing Rhodamine B degradation rate of 17  $\mu\text{m}$  long TNTs with space between tubes (75.9 %) to the 10  $\mu\text{m}$  long TNTs without space (67.5 %) (Table 2), it is so obvious that the space between tubes (i.e. inter-tube distance) can enhance the photocatalytic activity of TNTs.

### 3.2.3. Influence of the TNTs annealing temperature

To study the influence of annealing temperature on photocatalytic activity and the degradation of Rhodamine B prepared TNTs samples were annealed at 250 °C, 450 °C, 650 °C and 850 °C. Photocatalytic performance of TNTs with different dimensions and crystallinities are presented as degradation rate, rate constant and photonic efficiency and summarized in Table 2. The Table 2 and Fig. 10 presents results showing complete degradation of Rhodamine B on TNTs samples annealed at 250 °C, 450 °C and 650 °C along with colour removal within less than 180 minutes compared with 44.2 % degradation on the TNTs control sample (as produced at 25 °C). This enhancement of photocatalytic activity can be explained by significant influence of crystal structure of TNTs by thermal annealing. These results are consistent with XRD results (Fig. 5) which confirmed that by annealing the crystal structure of TNTs was changed from amorphous to crystalline anatase, rutile phase and their mixtures. It is previously reported that TiO<sub>2</sub> anatase phase has the highest photocatalytic activity compared with other phases. Interestingly, the results obtained in this study indicate that the anatase/rutile mixture of TiO<sub>2</sub> has higher photocatalytic activity than pure anatase phase. The TNTs annealed at 650 °C which has anatase/rutile mixture (86.5 % and 13.5% respectively) showed the fastest degradation rate since it had completely degraded the

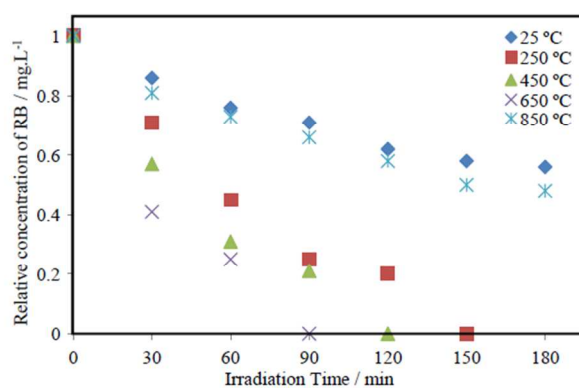


**Fig. 10** Removal of Rhodamine B under Hg (Xe) light irradiation by 45  $\mu\text{m}$  long TNTs; as produced (25 °C) and after annealing at different temperatures (250 °C, 450 °C, 650 °C and 850 °C).

Rhodamine B within 90 minutes followed by the TNTs annealed at 450 °C and 250 °C (100% anatase) (120 and 150 minutes respectively) (Table 2). The TNTs annealed at 850 °C which also has anatase/rutile mixture (12.1 and 87.9 % respectively) showed

the slowest degradation rate (51.6 %) among the annealed samples, which was similar to as produced amorphous TNTs (25 °C). This is explained by partial collapse of the TNTs tubular structure by annealing at temperature over 700 °C which is in agreement with previous studies.<sup>33</sup>

The kinetic study of Rhodamine B photodegradation reactions by TNTs is summarized in Figure 11. These graphs indicate the pseudo-first order reaction confirmed by a straight line of the log the Rhodamine B concentration versus degradation time gave.

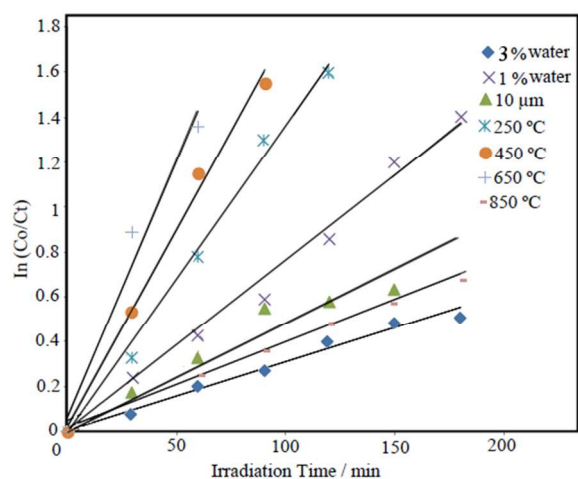


**Fig. 11** The semi-log graph of the degradation of Rhodamine B by different TNTs samples under Hg (Xe) light irradiation.

The slope of the linear regression equals the first order rate constant with an average coefficient value around 0.98. The rate constant ( $k$ ) of each reaction is calculated and subsequently used to calculate the photonic efficiencies. Table 2 summarizes reaction rate constant and photonic efficiency of TNTs with different dimensions, inter-tube distance and crystallinity. It is generally known that by increasing of the light intensity, the photonic efficiency decreased.<sup>34-35</sup> This is because at high light intensity the potential of electron-hole pair recombination is higher than electron-hole pair separation.<sup>29,36</sup> Therefore, the photonic efficiencies in this study could be improved by utilizing low photon flux in the photocatalytic process.

#### 4. Conclusion

The TNTs were prepared successfully using an electrochemical anodization approach. The presented results show that the nanotube's length, diameter and nanotube inter-distance and crystallinity can be adjusted by controlling the applied potential, anodization time, electrolyte water content and annealing temperature. Based on the results of the photodegradation experiments using Rhodamine B it is shown that the photocatalytic activity of TNTs is significantly affected by the structural and crystal properties of TNTs. Short tubes and larger inter-distance between nanotubes revealed higher photocatalytic activity than long and tightly packed TNTs. The annealing is shown to have most significance influence on photocatalytic properties with the highest performance of TNTs with

anatase/rutile mixture (86.5 % and 13.5 % respectively) prepared by annealing at 650 °C. In conclusion for the application of TNTs involving their photocatalytic requires it is important to consider of their dimensions and crystallinity which are controllable and can be optimised for specific application.

#### Acknowledgements

The authors acknowledge the facilities, and the scientific and technical assistance of the Australian Microscopy & Microanalysis Research Facility at the Electron Microscope Unit, The University of Adelaide. Mohammed Alsawat thanks Taif University (Ministry of Higher Education, Saudi Arabia) for funding his scholarship.

#### Notes and references

- <sup>a</sup> School of Chemical Engineering, The University of Adelaide, Adelaide, Australia. Fax: +61 8 8303 4373; Tel: +61 8 8313 4648;  
<sup>55</sup> E-mail: [dusan.losic@adelaide.edu.au](mailto:dusan.losic@adelaide.edu.au)  
<sup>b</sup> School of Chemical and Physical Sciences, Flinders University, Adelaide, Australia.
1. D. Ravelli, D. Dondi, M. Fagnoni, A.D. Albini, *Chemical Society Reviews*, 2009, **38**, 1999-2011
  2. M. Răileanu, M. Crișan, I. Nițoi, A. Ianculescu, P. Oancea, D. Crișan and L. Todan, *Water, Air, & Soil Pollution*, 2013, **224**, 1-45.
  3. M. N. Chong, B. Jin, C. W. Chow and C. Saint, *Water Research*, 2010, **44**, 2997-3027.
  4. M. Kaneko and I. Okura, *Photocatalysis: science and technology*, Springer, 2002.
  5. M. Zlámal, J. Krýsa and J. Jirkovský, *Catalysis letters*, 2009, **133**, 160-166
  6. J.-H. Lee, I.-C. Leu, M.-C. Hsu, Y.-W. Chung and M.-H. Hon, *The Journal of Physical Chemistry B*, 2005, **109**, 13056-13059.
  7. T. Kasuga, M. Hiramatsu, A. Hoson, T. Sekino and K. Niihara, *Langmuir*, 1998, **14**, 3160-3163.
  8. H.-H. Ou and S.-L. Lo, *Separation and Purification Technology*, 2007, **58**, 179-191.
  9. P. Roy, S. Berger and P. Schmuki, *Angew. Chem., Int. Ed.*, 2011, **50**, 2904-2939.
  10. J. Macak, H. Tsuchiya, A. Ghicov, K. Yasuda, R. Hahn, S. Bauer and P. Schmuki, *Current Opinion in Solid State and Materials Science*, 2007, **11**, 3-18.
  11. G. K. Mor, O. K. Varghese, M. Paulose, K. Shankar and C. A. Grimes, *Solar Energy Materials and Solar Cells*, 2006, **90**, 2011-2075.
  12. A. Ghicov and P. Schmuki, *Chemical Communications* 2009, 2791-2808.
  13. M. Sinn Aw, M. Kurian, D. Losic, *Biomaterials Science*, 2014, **2**, 10-34
  14. H.-F. Zhuang, C.-J. Lin, Y.-K. Lai, L. Sun and J. Li, *Environmental Science and Technology*, 2007, **41**, 4735-4740.
  15. J. Yu and B. Wang, *Applied Catalysis B: Environmental*, 2010, **94**, 295-302.
  16. J. M. Macak, M. Zlamal, J. Krysa and P. Schmuki, *Small*, 2007, **3**, 300-304.
  17. Y. Lai, L. Sun, Y. Chen, H. Zhuang, C. Lin and J. W. Chin, *Journal of the Electrochemical Society*, 2006, **153**, D123-D127.

18. H.-c. Liang and X.-z. Li, *Journal of Hazardous Materials*, 2009, **162**, 1415-1422.
19. K. Kant and D. Losic, *physica status solidi (RRL)-Rapid Research Letters*, 2009, **3**, 139-141.
20. K. Vasilev, Z. Poh, K. Kant, J. Chan, A. Michelmore and D. Losic, *Biomaterials*, 2010, **31**, 532-542
21. G. Oskam, A. Nellore, R. L. Penn and P. C. Searson, *The Journal of Physical Chemistry B*, 2003, **107**, 1734-1738.
22. R. A. Spurr and H. Myers, *Analytical Chemistry*, 1957, **29**, 760-762.
23. M. Muneer and D. Bahnemann, *Applied Catalysis B: Environmental*, 2002, **36**, 95-111.
24. Z. Su and W. Zhou, *Advanced Materials*, 2008, **20**, 3663-3667.
25. N. Vaenas, M. Bidikoudi, T. Stergiopoulos, V. Likodimos, A. G. Kontos and P. Falaras, *Chemical Engineering Journal*, 2013, **224**, 121-127
26. K. Lee, D. Kim, P. Roy, I. Paramasivam, B. I. Birajdar, E. Spiecker and P. Schmuki, *Journal of the American Chemical Society*, 2010, **132**, 1478-1479.
27. P. Qu, J. Zhao, T. Shen and H. Hidaka, *Journal of Molecular Catalysis A: Chemical*, 1998, **129**, 257-268.
28. A. Bhattacharyya, S. Kawi and M. Ray, *Catalysis Today*, 2004, **98**, 431-439.
29. I. K. Konstantinou and T. A. Albanis, *Applied Catalysis B: Environmental*, 2004, **49**, 1-14.
30. W. Z. Tang and H. An, *Chemosphere*, 1995, **31**, 4157-4170.
31. M. Saquib and M. Muneer, *Dyes and Pigments*, 2003, **56**, 37-49.
32. H. F. Zhuang, C. J. Lin, Y. K. Lai, L. Sun and J. Li, *Environmental Science and Technology*, 2007, **41**, 4735-4740.
33. Y. L. Pang, A. Z. Abdullah and S. Bhatia, *Applied Catalysis B: Environmental*, 2010, **100**, 393-402.
34. L. Zhang, W. A. Anderson and Z. J. Zhang, *Chemical Engineering Journal*, 2006, **121**, 125-134.
35. O. K. Dalrymple, D. H. Yeh and M. A. Trotz, *Journal of Chemical Technology and Biotechnology*, 2007, **82**, 121-134.
36. S. B. Kim and S. C. Hong, *Applied Catalysis B: Environmental*, 2002, **35**, 305-315.